Vol. 42 — N° 2 06 18 P. 239 – 251

GEOSTANDARDS and GEOANALYTICAL RESEARCH

Determination of Trace Elements in Bauxite Using Laser Ablation-Inductively Coupled Plasma-Mass Spectrometry on Lithium Borate Glass Beads

Dewany A. **Monsels** (1, 2)*, Manfred J. **Van Bergen** (1) and Paul R. D. **Mason** (1)

(1) Department of Earth Sciences, Utrecht University, Utrecht, The Netherlands
(2) Department of Geology and Mining, Anton de Kom University of Suriname, Paramaribo, Suriname
* Corresponding author. e-mail: dewany.monsels@uvs.edu, dewanymon@yahoo.co.uk

Quantification of trace element contents in bauxite by solution ICP-MS and other analytical methods that rely on conventional dissolution techniques can be challenging, because the refractory nature of common host minerals complicates complete digestion. Fusion with lithium borate, frequently used as a sample preparation method for XRF analysis of solid materials, avoids these problems. This manuscript documents that subsequent analysis of the low-dilution glass beads by laser ablation ICP-MS is a fast, accurate and precise method for determining trace element mass fractions in samples of bauxite and similar natural materials. The method was validated by determining thirty trace elements, including thirteen rare earth elements, in international reference materials for bauxite (ANRT BX-N, NIST SRM 69b, NIST SRM 696, NIST SRM 698) and iron formations (CCRMP FeR-2). Trace elements were typically measured to within 20% of reference values with an 'external' precision of < 20% RSD. Measurement results from various deposits in Suriname illustrate the procedure's effectiveness for studies concerning chemical properties and origin of bauxite.

Keywords: bauxite, trace elements, laser ablation, ICP-MS, lithium borate glass beads, reference materials, Suriname.

Received 02 Aug 17 – Accepted 14 Jan 18

Bauxite is the most important raw material for commercial aluminium production. The natural weathering processes that cause Al accumulation also promote enrichment of other relatively immobile constituents of original parent rocks. This happens to such an extent that waste products of industrial processing receive increasing attention as potential economic sources of trace elements, such as gallium, scandium and rare earth elements (Ochsenkühn-Petropoulou *et al.* 1994, Paramguru *et al.* 2004, Zhang *et al.* 2005, Borra *et al.* 2015, Ujaczki *et al.* 2017). Analysis of the major and trace element composition of bauxite not only serves to constraining ore grade but also provides information on parent rocks and the nature and conditions of genetic processes. This can be used as a guide for exploration or processing strategies. Trace element contents in bauxites have been determined by a variety of methods including instrumental neutron activation analysis (INAA) (Vukotić 1983, Korotev 1996, Grant *et al.* 2005), X-ray fluorescence spectrometry (XRF) (Mordberg *et al.* 2001) and inductively coupled plasma-atomic emission spectrometry (ICP-AES) (Boulangé and Colin 1994, Ochsenkühn-Petropoulou *et al.* 1990). In recent years, inductively coupled plasma-mass spectrometry (ICP-MS) has become the technique of choice because it allows the determination of a comprehensive set of elements that includes transition metals, high field-strength elements (HFSE) and rare earth elements (REE) at low mass fractions (e.g., Horbe and Anand 2011, Gu *et al.* 2013, Wang *et al.* 2013, da Costa *et al.* 2014, Mongelli *et al.* 2014, Ahmadnejad *et al.* 2017). However, a key concern in obtaining reliable trace element mass fractions by solution ICP-MS is the difficulty in achieving complete digestion of the bauxite, as it often contains refractory minerals such as zircon, anatase/rutile, monazite, xenotime, titanite, thorite and tourmaline (Bárdossy and Aleva 1990, Horbe and Da Costa 1999, da Costa *et al.* 2014, Monsels and Van Bergen 2017a, b). These are usually inherited from the parent rock and host many of the elements of interest.

Mixed acid attack may result in incomplete recoveries of analytes if resistant minerals are present, or as insoluble AlF_3 precipitates form that could incorporate significant amounts of trace elements (Yu *et al.* 2003, Cotta and Enzweiler

doi: 10.1111/ggr.12206

2011, Chen *et al.* 2017). Hence, special optimisation of the acid digestion method is recommended to accurately determine trace element contents of bauxite samples by ICP-MS (Zhang *et al.* 2016). An alternative method to ensure dissolution of refractory minerals is fusion with lithium borate followed by acid dissolution of the glass product (e.g., Panteeva *et al.* 2003, Yu *et al.* 2003, Awaji *et al.* 2006), with the additional advantage that the same sample can be analysed for major elements by XRF and for trace elements by ICP-MS (De Madinabeita *et al.* 2008, Amosova *et al.* 2016).

Although fusion treatment with an alkali flux is efficient in decomposing refractory minerals, typical drawbacks for ICP-MS are the introduction of a large amount of total dissolved solids (TDS) causing suppression/enhancement effects and extensive instrumental drift, relatively high blank levels, as well as a risk of contamination from impure reagents or metal crucibles (Totland and Jarvis 1993, Yu *et al.* 2003, Awaji *et al.* 2006).

Several of these problems are overcome when using laser ablation-inductively coupled plasma-mass spectrometry (LA-ICP-MS), which is a widely used technique for the microanalysis of solid materials and has been extensively tested for the analysis of XRF fusion beads (Nesbitt *et al.* 1997, Günther *et al.* 2001, Eggins 2003, Orihashi and Hirata 2003, Petrelli *et al.* 2007, Regnery *et al.* 2009, Leite *et al.* 2011, Park *et al.* 2016). The relatively small amount of solid particles introduced by this method are not susceptible to the same matrix effects as observed when aspirating solutions rich in lithium borate flux. LA-ICP-MS also offers several major advantages compared with more conventional analytical methods for the analysis of solid fusion beads such as XRF, including the multi-element determination capability coupled with high detection power. On the other hand, accuracy and precision in LA-ICP-MS can be limited by elemental fractionation at or close to the site of ablation, incomplete ionisation of the particles in the plasma, relatively poor stability of the plasma source, spectroscopic interferences, difficulties in correcting for ablation yield and the lack of suitable matrix-matched reference materials (e.g., Longerich *et al.* 1996, Mason and Kraan 2002, Yu *et al.* 2003, Jochum *et al.* 2007, Regnery *et al.* 2009, Miliszkiewicz *et al.* 2015, Shazzo and Karpov 2016, Zhang *et al.* 2016, Chen *et al.* 2017).

In this study, we investigate the utility of laser ablation ICP-MS after lithium borate fusion for bauxite analysis. The method was validated using international reference materials for bauxite and iron formation, as well as USGS basaltic glass BCR-2G as a control reference material.

Experimental procedure

Materials

Four international geological reference materials for bauxite, NIST SRM 69b (Arkansas, USA), NIST SRM 696 (Suriname), NIST SRM 698 (Jamaica) and BX-N (France) were prepared as lithium borate glasses following conventional sample preparation procedures for XRF analysis. An iron formation reference material (FeR-2 from Canada) was prepared in the same way to account for possible Fe enrichments in the bauxite profiles. The glass beads were prepared by mixing 1 g of ignited reference material powder with 4 g of flux consisting of 66.5% *m/m* lithium tetraborate ($Li_2B_4O_7$) and 33.5% *m/m* lithium metaborate ($LiBO_2$). The mixture was heated in a platinum crucible (75% Pt – 25% Au) at *ca.* 1100 °C and quenched into a platinum mould. Samples of Surinamese bauxite deposits were treated in the same way.

Analytical methods

Laser ablation analysis: Trace elements were determined by laser ablation-inductively coupled plasma-mass spectrometry (LA-ICP-MS) using a ThermoFischer Scientific Element 2 magnetic sector field ICP-MS instrument, coupled to a Lambda Physik excimer laser (193 nm) with GeoLas optics (Mason and Kraan 2002). Ablation parameters and operating conditions are given in Table 1. Calibration was performed against NIST SRM 612 following the methodology of Longerich *et al.* (1996) with double-standard measurements bracketing each of six unknown samples. Silicon

Table 1.
ICP-MS and laser ablation operating parameters

ICP-MS	
Plasma power	1300 W
Gas flows	
Cool	16 l min^{-1} Ar
Auxiliary	1.0 l min^{-1} Ar
Carrier	0.685 l min^{-1} Ar, 0.696 l min^{-1} He
Internal standard	^{29}Si
Laser	
Wavelength	193 nm
Pulse rate	10 Hz
Energy density at target	5 J cm^{-2}
Ablation crater diameter	120 µm
Ablation time	Total of 60 s + 30 s gas blank

(^{29}Si) was adopted as internal standard element using the recommended values for SiO_2 of 7.4, 3.79, 0.68, 13.41 and 49.24% *m/m* for BX-N, NIST SRM 696, NIST SRM 698, NIST SRM 69B and FeR-2 (Govindaraju 1994), respectively. Reported compositions are averages of three measurements for each sample.

Quality control: Accuracy was monitored by analysing USGS basaltic glass BCR-2G after each batch of six samples (Gao *et al.* 2002, Jochum *et al.* 2005, 2016). The compilation values of Govindaraju (1994, 1995) were used for the bauxite and iron formation reference materials. The available information for the BX-N and FeR-2 reference materials includes sets of recommended and provisional values, whereas no uncertainty information on the trace element working values was reported for the reference materials NIST SRM 69b, NIST SRM 696 and NIST SRM 698. For FeR-2, we also used a set of compilation values that were certified or provisionally recommended by the Canadian Certified Reference Materials Project (CCRMP) under the auspices of Natural Resources Canada (NRCan). Additional literature data included for comparison are solution ICP-MS values reported for the three NIST RMs (Wang *et al.* 2013) and FeR-2 (Yu *et al.* 2003, Sampaio and Enzweiler 2015) and INAA data for BX-N (Bédard and Barnes 2002), NIST SRM 69b (Korotev 1996), NIST SRM 696 and NIST SRM 698 (Grant *et al.* 2005). All reference data were extracted from the GeoReM database.

Table 2.
Summary of replicate analyses of USGS BCR-2G glass compared with GeoReM preferred values and other LA-ICP-MS results

m/z	Element	Measured (this work)[a]		GeoReM values[b] Jochum *et al.* (2016)		Other LA-ICP-MS results			% dev.		
						Gao *et al.* (2002)		Jochum *et al.* (2005)			
		µg g^{-1}	% RSD	µg g^{-1}	Uncertainty 95%CL	Mean (µg g^{-1})	% RSD	Mean (µg g^{-1})	GeoReM values	Gao *et al.* (2002)	Jochum *et al.* (2005)
45	Sc	34.4	7	33.53	0.4	32	6		3	8	
51	V	466	6	417.6	4.5	425	2		12	10	
52	Cr	17.4	8	15.85	0.38	17	12		10	2	
66	Zn	134	13	129.5	1.8	153	6		4	-12	
75	As	1.09	13	0.86	0.22	-	-		27	-	
85	Rb	48.7	3	46.02	0.56	51	6	45.1	6	-4	8
88	Sr	323	6	337.4	6.7	321	2	332	-4	0.6	-3
89	Y	33.6	8	36.07	0.37	31	6	36.9	-7	9	-9
90	Zr	179	12	186.5	1.5	167	5	188	-4	7	-5
93	Nb	11.4	5	12.44	0.2	10.9	6	12.3	-8	5	-7
133	Cs	1.13	7	1.16	0.023	1.17	7	1.1	-2	-3	3
137	Ba	698	8	683.9	4.7	641	2	650	2	9	7
139	La	24.5	6	25.08	0.16	25	4	25.5	-2	-2	-4
140	Ce	51.9	5	53.12	0.33	52	4	50.4	-2	-0.2	3
141	Pr	6.20	5	6.827	0.044	6.3	6	6.59	-9	-2	-6
146	Nd	27.4	6	28.26	0.37	27	4	28.5	-3	1.5	-4
147	Sm	6.33	7	6.547	0.047	6.3	8	6.58	-3	0.5	-4
151	Eu	1.83	6	1.989	0.024	1.91	5	1.95	-8	-4	-6
157	Gd	6.40	8	6.811	0.078	6.5	9	6.74	-6	-2	-5
159	Tb	0.95	9	1.077	0.026	0.95	7	1.07	-12	-0.2	-11
163	Dy	6.24	8	6.424	0.055	6	7	6.59	-3	4	-5
165	Ho	1.22	9	1.313	0.011	1.2	6	1.34	-7	2	-9
166	Er	3.54	9	3.67	0.038	3.3	6	3.76	-4	7	-6
172	Yb	3.34	8	3.392	0.036	3.2	9	3.59	-2	4	-7
175	Lu	0.48	8	0.5049	0.0078	0.47	9	0.531	-5	2	-10
178	Hf	4.66	12	4.972	0.034	4.5	9	5.07	-6	3	-8
181	Ta	0.70	4	0.785	0.018	0.63	10	0.761	-11	11	-8
208	Pb	11.5	23	10.59	0.17	10.9	5	10.6	8	5	8
232	Th	5.55	7	5.828	0.05	5.5	4	6.12	-5	1.0	-9
238	U	1.58	4	1.683	0.017	1.7	5	1.67	-6	-7	-5

Measured values based on Si as internal standard using SiO_2 = 54.00% *m/m* from Jochum *et al.* (2016). [a] Average of sixty-one spot measurements taken in five different sessions. [b] Reference values, except for As, La and Ho which are information values. Measurement uncertainties for the GeoReM values expressed at the 95% confidence level (CL).

Results and discussion

Heterogeneity testing was carried out on the fused lithium borate glass beads. Measurement precisions from multiple spot analyses in the individual glass beads are a guide for the degree of homogeneity, provided that uncertainties caused by counting statistics can be ignored. Average precisions for three independent spot analyses made on each of the five discs were better than 4% RSD, except for Rb, Cs and Zn (average 6–8% RSD), which are present in mass fractions relatively close to detection limits. This finding demonstrates a homogeneous distribution of analytes in the glasses.

In a separate run, we also examined possible uncertainties from the preparation procedure by measuring the element mass fractions in a set of five beads (six analysis spots each) prepared from a single bauxite sample (SNE-3135, Monsels and Van Bergen 2017a) using an automated casting device. The measurement repeatability, expressed as % RSD, was 5–10% for Sr, Y, La, Sm, Eu, Tb, Gd, Er, Lu, Pb and 10–21% for the remaining trace elements, based on SiO_2 (0.50% *m/m*) as internal standard. No systematic relationship between RSD and mass fraction levels was observed.

The average relative standard deviation (RSD) of the elements measured in the BCR-2G basaltic glass reference material (Table 2), used to monitor instrumental and procedural performance, was typically better than 10%, except for Zn, As, Zr, Hf (12–13%), whereas precision was relatively poor for Pb (23%). Accuracy, measured against the GeoReM results (Jochum *et al.* 2016) was excellent. The deviation from recommended values, determined in multiple sessions, was ≤ 12% for all reported trace elements in BCR-2G (Figure 1), except for As, which is present at a level of *ca.* 1 μg g^{-1}. Comparison with other LA-ICP-MS results obtained on BCR-2G (Gao *et al.* 2002, Eggins 2003, Jochum *et al.* 2005, Andrade *et al.* 2014) also shows good agreement.

A rigorous assessment of the quality of our data obtained on the reference bauxites and iron formation was hampered by the lack of certified/recommended values for trace elements in these materials. Reference BX-N is the only bauxite reference material with a virtually complete set of recommended or provisional values available for comparison (Govindaraju 1994, 1995). Relative to these data, our results generally show good agreement (Tables 3–5 and Figure 2). Relative deviations (% dev) are better than 10% for Zn, Sr, Y, Zr, Nb, most of the REE, Hf, Pb and Th, while % dev. values are between 10 and 20% for As, Rb, Ba, Eu, Gd, Tb, Ho, Ta and U. Poor accuracy (% dev. > 20) is shown by Sc, V, Cr and Cs.

The iron formation reference material FeR-2 has a substantially different trace element composition, as it contains some 40 times less As, 10–20 times less REE and HFSE, two to five times less Zn, Sr, Eu, Cr and seven to twenty times more Ba, Cs and Rb than BX-N (Table 5). Nonetheless, relative to recommended or provisional values (Govindaraju 1994, 1995), our results for FeR-2 show roughly the same levels of accuracy as for BX-N with deviations strongly dependent on mass fraction.

Comparison with the available INAA data on the bauxite reference materials BX-N, NIST SRM 69b, NIST SRM

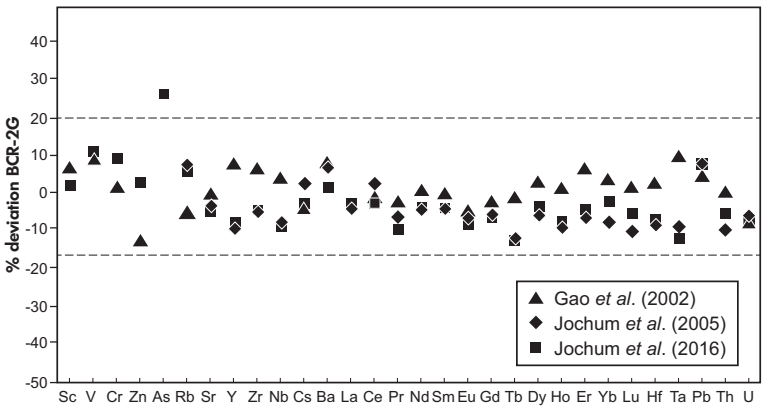

Figure 1. Comparison of trace element mass fractions measured by LA-ICP-MS in BCR-2G relative to GeoReM values (Jochum *et al.* 2016) and other LA-ICP-MS results (Gao *et al.* 2002, Jochum *et al.* 2005), expressed as per cent difference (% dev.). The measured mass fractions (Table 2) are averages of sixty-one spot analyses obtained during five different measurement sessions.

Table 3.
Measured values of ANRT BX-N and NIST SRM 69b compared with reference values

Element	ANRT BX-N										NIST SRM 69b											
	Measured (this work)			Govindaraju (1994)				Bédard and Barnes (2002)			Measured (this work)			Govindaraju (1994)			Korotev (1996)			Zhang *et al.* (2016)		
	µg g^{-1}	1*s* (*n* = 3)	% RSD	Compiled µg g^{-1}	± 1*s*		% dev.	INAA µg g^{-1}	± 1*s*	% dev.	µg g^{-1}	1*s* (*n* = 3)	% RSD	Compiled µg g^{-1}		% dev.	INAA µg g^{-1}	95% CL (rel)	% dev.	ICP-MS aver-age	1*s* (*n* = 3)	% dev.
Sc	72.1	1.8	2.4	60	10	R	20	61.55	0.09	17	15.5	0.7	4.5	8	R	93	8.32	3	86			
V	435	4	0.9	350	77	P	24				167	3	1.8	160	R	4				147	8	13
Cr	346	2	0.5	280	75	R	24	290	2	19	86.1	2.0	2.2	75	R	15	73	10	18	59.8	3	44
Zn	81.7	3.1	3.8	80	39	R	2				36.5	4.6	12	28	R	30				21.2	1	72
As	131	6	5.0	115	9	R	14	120.5	1	8	26.2	0.2	0.9				24.4	3	8			
Rb	2.91	0.08	2.8	3.6	11	P	-19				3.52	0.17	4.6				4.4	30	-20	3.33	0.03	6
Sr	109	1	0.9	110	19	P	-1				126	2	1.6				134	10	-6	126	4	0.1
Y	118	2	1.5	114	40	P	3				67.2	0.68	1.0				78	-	-14	69.0	1	-3
Zr	564	8	1.3	550	89	P	2				2882	20.6	0.7	2150	R	34	2670	10	8	2632	39	10
Nb	54.5	0.8	1.5	52	5	P	5				861	5	0.5							868	8	-1
Cs	0.30	0.02	7.9	0.4	-	R	-24				0.09	0.02	17				0.15	30	-38	0.15	0.01	-36
Ba	33.4	0.2	0.5	30	26	P	11				78.7	1.8	2.2	72	R	9	77	30	2	78.0	4	1
La	377	5	1.3	355	76	R	6	386.5	0.7	-3	81.4	1.4	1.7				75	3	8	72.2	4	13
Ce	558	2	0.4	520	43	R	7	574	2	-3	241	4	1.4	240	R	1	249	3	-3	242	2	-0.3
Pr	51.2	0.4	0.8	54	-	R	-5				10.5	0.2	1.6							10.6	0.3	-0.1
Nd	156	1	0.9	163	31	R	-4	178	2	-12	31.5	0.7	2.1				31	10	2	31.0	1	2
Sm	21.0	0.3	1.5	22	3.4	R	-5	22.64	0.03	-7	5.37	0.06	1.1				5.73	3	-6	5.70	0.3	-6
Eu	3.98	0.10	2.6	4.4	0.5	R	-10	4.44	0.2	-10	0.79	0.02	2.6				0.866	3	-9	0.84	0.03	-6
Gd	17.4	0.3	1.7	20	6.4	R	-13				5.26	0.02	0.4				5.7	-	-8	5.80	0.3	-9
Tb	2.67	0.02	0.9	3	0.3	R	-11	3.15	0.1	-15	1.07	0.01	0.6				1.21	10	-11	1.23	0.04	-12
Dy	18.6	0.1	0.7	18.5	-	R	1				8.99	0.21	2.2				9.2	-	-2	9.40	0.2	-4
Ho	3.67	0.07	1.8	4.1	-	R	-10				2.08	0.05	2.5				2.4	-	-13	2.25	0.1	-8
Er	11.0	0.1	0.6	11	-	R	0.2				7.65	0.16	2.0				8	-	-4	7.71	0.2	-1
Yb	11.9	0.4	3.1	11.6	2.1	R	3	12.4	0.1	-4	10.5	0.3	2.5				10.4	10	1	10.4	0.4	1
Lu	1.67	0.06	3.3	1.8	0.4	R	-7	1.89	0.02	-12	1.54	0.03	2.0				1.58	10	-3	1.56	0.1	-1
Hf	13.9	0.2	1.7	15.2	4	P	-9	15.6	0.3	-11	52.1	1.4	2.5	63	R	-17	58.2	10	-10	54.1	3	-4
Ta	3.7	0.05	1.3	4.6	0.8	R	-19	4.2	0.2	-11	41.5	0.5	1.3				43.9	3	-6	45.1	1	-8
Pb	129	2	1.7	135	76	R	-4				41.2	0.8	1.8							47.2	3	-13
Th	46.4	0.5	1.0	50	11	P	-7	54.1	0.2	-14	79.4	1.4	1.7				83.9	3	-5	83.5	4	-5
U	7.83	0.07	0.9	8.8	2.4	P	-11	10	0.2	-22	10.8	0.2	1.8				12.9	-	-16	12.8	0.4	-15

Trace element mass fractions (µg g^{-1}) and precisions expressed as 1s and % RSD for LA-ICP-MS measurements on lithium borate glass beads, compared with reference values obtained by compilation, INAA or solution ICP-MS. he standard deviation values for measured mass fractions are based on three spot analyses on the same lithium borate glass bead. % dev. values represent relative difference between measured and reference mass fractions expressed as a percentage. R (recommended value) and P (provisional value) (Govindaraju 1994, 1995).

Table 4.
Measured values of NIST SRM 696 and NIST SRM 698 compared with reference values

Element	NIST SRM 696										NIST SRM 698									
	Measured (this work)			Govindaraju (1994)		Grant *et al.* (2005)		Zhang *et al.* (2016)			Measured (this work)*			Govindaraju (1994)		Grant *et al.* (2005)		Zhang *et al.* (2016)		
	μg g^{-1}	1*s* (*n* = 3)	% RSD	Compiled μg g^{-1}	% dev.	INAA μg g^{-1}	% dev.	ICP-MS		% dev.	μg g^{-1}	1*s* (*n* = 3)	% RSD	Compiled μg g^{-1}	% dev.*	INAA μg g^{-1}	% dev.	ICP-MS		% dev.
								average	1*s* (*n* = 3)									Average	1*s* (*n* = 3)	
Sc	12.1	0.9	7.6	8	51	8.2	47				52.1	0.8	1.5	51	2	51.1	2			
V	447	6	1.4	400	12	383.8	16	381	6	17	363	2	0.4	360	1	342.5	6	339	13	7
Cr	362	2	0.7	320	13	310.3	17	288	7	26	562	3	0.4	550	2	513.8	9	502	5	12
Zn	17.7	3.0	17	11	61	11.7	51	6.30	0.20	181	182	2	1.3	230	-21	232.1	-21	268	3	-32
As	14.9	0.4	3.0			14.4	4				38.1	0.7	1.9			39.9	-5			
Rb	0.40	0.02	4.0					0.31	0.01	30	0.67	0.13	19					0.61	0.02	9
Sr	21.5	0.6	2.6			179.5	-88	21.1	0.3	2	124	2	2.0			308.3	-60	152	3	-19
Y	13.4	0.4	2.6					14.5	1.1	-8	252	3	1.0					313	8	-20
Zr	1076	10	1.0	1040	3			1023	13	5	427	5	1.2	450	-5			482	9	-12
Nb	51.4	1.0	2.0					53.5	0.5	-4	44.0	1.0	2.2					53.4	2	-18
Cs	0.04	0.001	2.0			0.2	-82	0.030	0.003	17	0.14	0.01	10			0.9	-84	0.20	0.01	-28
Ba	12.6	0.8	6.2	36	-65			12.5	0.3	1	44.9	1.0	2.3	72	-38			63.7	2	-30
La	29.9	0.8	2.7			26.4	13	23.8	0.3	26	226	4	1.6			272.2	-17	257	5	-12
Ce	36.2	1.1	2.9	41	-12	42.1	-14	36.1	0.1	0.5	251	8	3.0	300	-16	293.2	-14	290	2	-14
Pr	3.30	0.08	2.5					3.26	0.0	1	33.8	1.0	2.8					40.9	1	-18
Nd	10.4	0.4	3.6			9.4	10	10.2	0.1	1	134	3	2.5			233	-43	160	2	-17
Sm	1.72	0.05	2.6			2.1	-18	1.76	0.04	-2	22.7	0.5	2.2			30.3	-25	28.8	1	-21
Eu	0.33	0.02	6.0			0.5	-33	0.37	0.01	-10	5.12	0.19	3.6			5.8	-12	6.25	0.04	-18
Gd	1.41	0.09	6.5					1.41	0.03	-0.1	24.0	0.7	3.1					24.2	0.3	-1
Tb	0.25	0.01	4.6			0.3	-16	0.28	0.01	-9	3.30	0.07	2.1			3.7	-11	4.46	0.0	-26
Dy	2.01	0.08	4.0			2.1	-4	2.11	0.07	-4	23.2	0.7	3.1			29.8	-22	28.5	0.4	
Ho	0.46	0.03	5.5					0.48	0.02	-3	4.78	0.16	3.3					6.04	0.1	-21
Er	1.57	0.08	5.1					1.58	0.06	-1	13.1	0.4	2.9					15.7	0.2	-17
Yb	2.24	0.12	5.4			3.4	-34	2.25	0.08	0	10.3	0.3	2.9			9.2	12	12.2	0.4	-15
Lu	0.35	0.01	3.9			0.4	-12	0.39	0.01	-9	1.38	0.03	2.1			1.8	-23	1.70	0.1	-19
Hf	24.6	1.1	4.3	32	-23	34.8	-29	29.0	1.6	-15	10.5	0.3	2.9	15	-30	14.1	-25	14.3	0.1	-26
Ta	3.75	0.20	5.2					4.19	0.10	-10	2.84	0.14	4.7					3.72	0.1	-24
Pb	18.1	1.1	6.1					21.5	0.41	-16	59.1	2.8	4.7					85.5	1	-31
Th	62.2	2.5	4.1			77.5	-20	70.4	0.9	-12	26.5	1.0	3.7			34.7	-24	32.5	2	-18
U	4.01	0.20	4.9			5.1	-21	4.72	0.07	-15	6.81	0.25	3.6			9.8	-31	9.55	0.2	-29

See Table 3 for explanation.

Table 5.
Measured values of FeR-2 compared with reference values

Element	CCRMP FeR-2												
	Measured (this work)			Govindaraju (1994)			ICP-MS			% dev.	CCRMP		
	μg g^{-1}	1*s* (*n* = 3)	% RSD	Compiled μg g^{-1}		% dev.	Average	1*s*	*n*		Compiled μg g^{-1}		% dev.
Sc	10.0	0.3	2.9	6	P	67	5.55	0.34	2	80	6	C	67
V	50.0	0.5	0.9	36	R	39	34.5	6.4	2	45	37	C	35
Cr	62.1	0.9	1.4	46	R	35	45.5	2.1	2	36	47	C	32
Zn	39.6	0.5	1.2	44	R	-10	36.5	0.7	2	8	43	C	-8
As	3.14	0.2	7.6	2.1	P	49		-			2	PR	57
Rb	62.7	0.2	0.3	67	P	-6	64.3	3.5	2	-2	66	C	-5
Sr	60.2	1.3	2.2	58	R	4	64.0	3.2	4	-6	58	C	4
Y	13.8	0.3	2.3	16	R	-13	12.7	1.1	5	9	15	C	-8
Zr	40.7	0.8	2.0	39	R	4	39.8	4.1	4	2	39	C	4
Nb	4.24	0.08	1.8				3.01	0.65	4	41			
Cs	4.21	0.05	1.2	4.5	P	-6	4.89	0.08	2	-14	5	PR	-16
Ba	216	3	1.6	230	R	-6	227	17	4	-5	240	PR	-10
La	22.8	0.4	1.9	12	P	90	12.4	0.71	5	84	14	C	63
Ce	23.5	0.4	1.6	25	R	-6	25.2	1.79	5	-7			
Pr	2.75	0.08	2.9	3	P	-8	3.04	0.20	5	-9			
Nd	11.7	0.2	2.1	12	P	-3	12.3	0.93	5	-5			
Sm	2.54	0.15	6.0	2.5	R	2	2.60	0.28	5	-2	2.6	C	-2
Eu	1.23	0.05	4.3	1.25	P	-1	1.29	0.12	5	-4			
Gd	2.17	0.08	3.6	2	R	8	2.37	0.30	5	-9			
Tb	0.32	0.02	4.9	0.32	P	-1	0.36	0.03	5	-11			
Dy	2.24	0.17	7.5	2	P	12	2.27	0.19	5	-1			
Ho	0.46	0.01	3.0	0.6	P	-23	0.48	0.05	5	-4			
Er	1.40	0.08	5.8	1.5	P	-7	1.44	0.14	5	-2			
Yb	1.39	0.03	1.8	1.25	R	11	1.38	0.15	5	1	1.3	C	7
Lu	0.20	0.01	7.0	0.2	P	-2	0.21	0.02	5	-5			
Hf	0.98	0.04	3.7	1	P	-2	1.16	0.13	4	-15			
Ta	0.18	0.01	3.3	0.2	P	-10	0.21	0.04	4	-12			
Pb	7.61	0.08	1.1	11	P	-31	8.92	0.62	4	-15	11	C	-31
Th	2.41	0.09	3.8	2.4	P	0	2.77	0.35	4	-13	3	C	-20
U	0.94	0.04	4.3	1.2	P	-22	1.08	0.17	4	-12			

See Table 3 for explanation.

696 and NIST SRM 698 yields an ambiguous picture. For virtually all elements, our results show excellent agreement with the data for BX-N and NIST SRM 69b reported by Bédard and Barnes (2002) and Korotev (1996), respectively. In contrast, relative to the results for NIST SRM 696 and NIST SRM 698 of Grant *et al.* (2005), many of our measurement results deviate substantially (% dev. values are > 20 for some 30% of the elements).

In general, our results compare well with solution ICP-MS data that cover a more complete set of trace elements than the INAA data. With the exception of a few elements, there is excellent correspondence with the solution ICP-MS data for NIST SRM 69b and NIST SRM 696 (Zhang *et al.* 2016) and for FeR-2 (Yu *et al.* 2003, Sampaio and Enzweiler 2015). Only for NIST SRM 698 (Zhang *et al.* 2016), our results are consistently *ca.* 17% lower, comparable to the average difference with the INAA data of Grant *et al.* (2005). We attribute the systematic offsets for this reference to its low Si content (0.68% *m/m* SiO_2, Govindaraju 1994), which may have affected the use of this element as internal standard, either due to analytical uncertainty in the recommended value for this bauxite reference material, or to the low count-rate ratio of 1.8 for the pre-ablation blank and the analyte signal recorded in our measurement. When adopting Ce as internal standard for the NIST SRM 698 measurement and using the compilation value of 300 μg g^{-1} of Govindaraju (1994), the agreement with the solution ICP-MS results of Zhang *et al.* (2016) becomes excellent for some 90% of the trace elements determined (Table 4 and Figure 2).

Sources of error

Sources of analytical error that potentially affected the results are either inherent to the ICP-MS technique or specifically associated with the use of borate glasses. Explanations for the frequent, relatively large deviations of measured mass fractions of some elements (e.g., Sc, V, Cr, Zn,

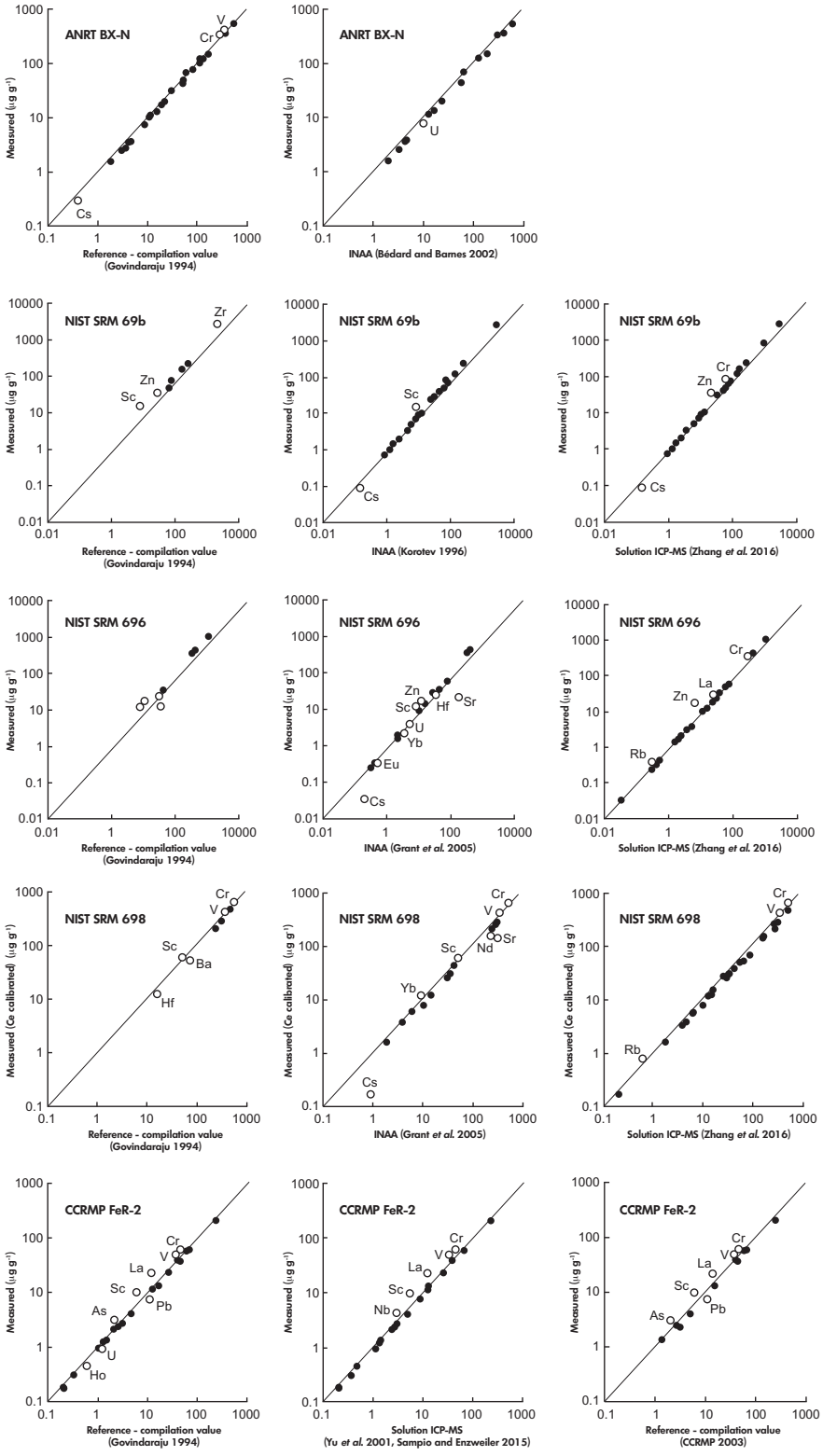

Figure 2. Comparison of LA-ICP-MS results with reference values, INAA data and solution ICP-MS data for international reference bauxites and iron formation (see Tables 3–5 and text for discussion). Labelled open symbols indicate measurement results with relatively large deviations (> 20%) from comparison values. Plotted results for measurements on NIST SRM 698 are based on Ce as internal standard (value from Govindaraju 1994) instead of Si (see text).

La, Pb) compared with reported values may include contamination or loss during sample preparation, impurities in the borate flux and polyatomic spectral interferences. The persistently overestimated mass fractions of Sc, V, Cr are likely attributable to polyatomic interferences, which is a well-known problem in ICP-MS analysis of these elements (Evans and Giglio 1993, May and Wiedmeyer 1998, Reed *et al.* 1994). Relative to the working values of Govindaraju (1994, 1995) for the analysed reference materials, the measured Sc values are 47–93% too high at low mass fractions (< 10 μg g^{-1}), whereas they are much closer (≤ 20%) at elevated mass fractions (> 50 μg g^{-1}). Numerous polyatomic ions with a mass over charge ratio (*m/z*) of 45 could interfere on ^{45}Sc (e.g., Whitty-Léveillé *et al.* 2016) and may thus contribute to this overestimation. They include silicon-based ions ($^{29}Si^{16}O^+$, $^{28}Si^{17}O^+$, $^{28}Si^{1}H^{16}O^+$) and ions that may be produced from lithium borate constituents (e.g., $^{7}Li^{38}Ar^+$, $^{1}H_2{}^{16}O_2{}^{11}B^+$, $^{1}H_3{}^{16}O_2{}^{10}B^+$). In addition, doubly charged Zr atoms ($^{90}Zr^{2+}$) may add to the interference problem on ^{45}Sc. The high Zr mass fractions in the bauxite reference materials (427–2882 μg g^{-1}) and a clear correlation between Zr and % dev. values for Sc in our results suggest that this might be the case. Whitty-Léveillé *et al.* (2016) used mass filtering techniques in tandem quadrupole ICP-MS to reduce Si-, B- and Zr-based interferences on ^{45}Sc. Similar to our results, they measured a high apparent Sc mass fraction of 76 ± 5 μg g^{-1} for lithium metaborate-fused BX-N by conventional quadrupole solution ICP-MS, but obtained an accurate and precise result (60 ± 2 μg g^{-1}) relative to the expected value of Govindaraju (1994) after interference removal.

Largest deviations from expected values at lowest mass fractions are also observed for V (% dev. > 30 at < 50 μg g^{-1})

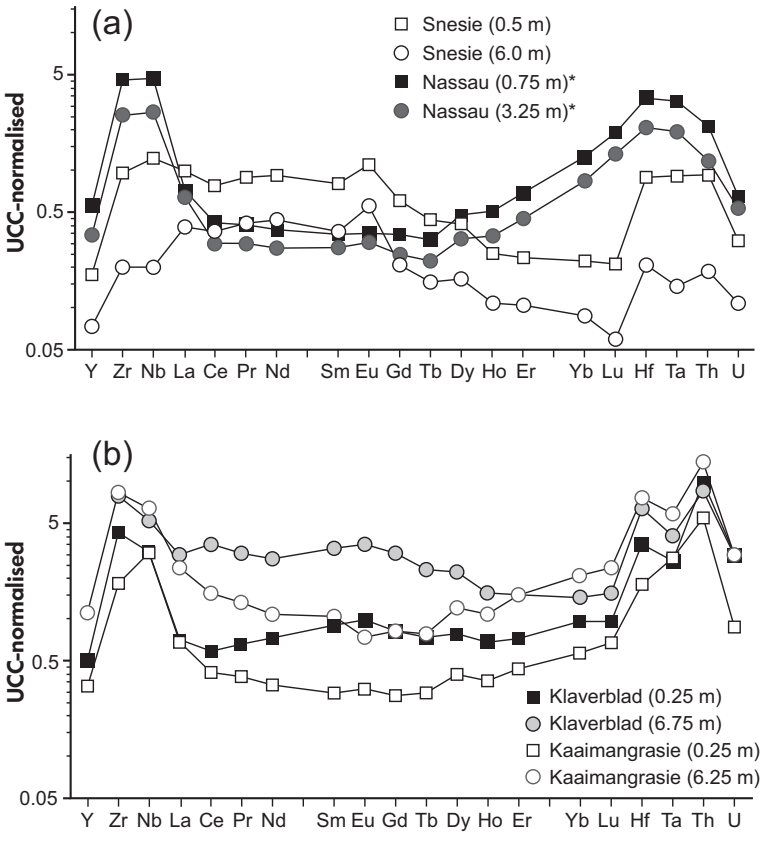

Figure 3. Trace element abundances of HFSE and REE, normalised to upper continental crust (UCC, McLennan 2001) in selected samples from four bauxite deposits in Suriname (see Monsels 2016, Monsels and Van Bergen 2017a, b, for locations) to illustrate the applicability of LA-ICP-MS on lithium borate glass beads for bauxite analysis. (a) Samples from the top (squares) and bottom parts (circles) of bauxite profiles on Proterozoic crystalline parent rocks (see text); data from Monsels and Van Bergen (2017a). (b) Samples from the top (squares) and bottom parts (circles) of bauxite profiles on Tertiary sediments; data from Monsels and Van Bergen (2017b). *Note that La mass fractions in the Nassau samples are overestimated due to impurity of the borate flux.

and Cr (% dev. > 30 at < 70 μg g^{-1}), both in FeR-2. Possible interference effects include those of $^{11}B^{40}Ar^{+}$ on $^{51}V^{+}$ and Ar-based species (e.g., $^{36}Ar^{16}O^{+}$) on ^{52}Cr. The results for As agree well with literature data except for a ca. 50% overestimation relative to the provisionally recommended low value of 2 μg g^{-1} in FeR-2. Other common interferences (e.g., oxides of Ba and light REE on middle and heavy REE) were probably insignificant, given the overall good correspondence between measured and expected values for REE that are sensitive to this problem.

Substantial overestimation of La at low expected mass fractions (e.g., 60–90% at 12 μg g^{-1} for FeR-2) is most likely attributable to impure flux material. We noticed that batches of borate flux might contain detectable amounts of lanthanum despite its absence on the list of contaminants provided by the manufacturer. Test measurements on blanks prepared with one of the flux batches we used confirmed the presence of small amounts of La. Similar problems from flux impurities were reported by Eggins (2003) and Yu *et al.* (2003). However, analysis of blank glass beads, prepared from a different batch of borate flux to investigate possible impurity effects for the full range of elements, showed no excess La. Average count rates obtained on four borate beads, after subtraction of the gas blanks, were insignificant compared with those of the BX-N reference material (1.4–1.6% for Zn, Cs and Ba, 0.1–0.8% for Si, Sc, Cr, Rb, Sr, Eu, Gd, Lu and ≤ 0.1% for the other elements including La), which suggests that contributions from impurities are negligible when measuring bauxite in this borate flux. Our findings thus confirm that potential contaminants in flux material may vary in amount and require attention in each individual case. Low Pb mass fractions compared with expected values (% dev. values from -4 to -31) are possibly due to volatilisation during fusion. Petrelli *et al.* (2007) suggested that the amount of Pb loss could be related to the SiO_2 content of the sample.

A systematic error affecting all elements measured may arise from the choice of the internal standard. The use of ^{29}Si in this work was adequate, but SiO_2 contents in bauxite are sometimes very low (< 1% *m/m*), affecting accuracy in routine XRF analysis of fusion beads. In such cases, alternative elements can be used for this purpose (e.g., Fe), provided that they produce sufficiently high count rates to overcome background counting statistic limitations.

Application to Surinamese bauxites

Lateritic bauxite deposits in Suriname formed on a large diversity of precursor rocks, ranging from Proterozoic metamorphic crystalline basement rocks on plateaus in the country's interior to Tertiary continent-derived sediments in coastal lowlands (Bárdossy and Aleva 1990, Monsels 2016). Trace element abundances (Topp *et al.* 1984, Butt 1986, Monsels and Van Bergen 2017a, b) tend to be unique for each deposit as is illustrated for REE and HSFE distributions normalised to upper continental crust values (McLennan 2001) in Figure 3a and b.

Samples taken at two different depth levels in each of the vertical bauxite profiles display largely coherent patterns but different mass fractions. The patterns of the two bauxites that developed on the Proterozoic parent rocks are clearly different (Figure 3a). The Nassau profile on a low-grade metabasalt/andesite is marked by strong enrichments of HFSE relative to REE and heavy REE (HREE) relative to light REE (LREE). In contrast, the samples from the Snesie profile, developed on a high-grade metamorphic gneissic precursor, show elevated LREE/HREE ratios, a strong enrichment of HREE over HFSE and a conspicuous positive Eu anomaly. Likewise, bauxites from the two profiles on Tertiary sediments are compositionally distinct (Figure 3b). The REE part of the patterns shows a concave upward trend in the Kaaimangrasie samples and a concave downward trend in the Klaverblad samples, whereas in both cases, the HFSE are enriched and mass fraction differences between samples from different depths are much larger for REE than for HFSE. A combination of factors is inferred to be responsible for distinct trace element signatures observed, including the lithology of the parent rock, the history and controls of the weathering process, mobility of the REE and the nature of mineral hosts (Monsels and Van Bergen 2017a, b). These examples demonstrate the versatility of the routine described here for trace element determination in bauxite studies.

Conclusions

Laser ablation ICP-MS analysis of lithium borate glass beads was investigated for trace element measurements in bauxite using international reference materials (ANRT BX-N, NIST SRM 69b, NIST SRM 696, NIST SRM 698 and CCRMP FeR-2). Based on a comparison of our results with reference values and literature data, the technique enables the fast, accurate and precise determination of trace elements in bauxite samples, in particular for the HSFE and REE.

The lithium borate fusion procedure avoids sample decomposition problems associated with acid dissolution of refractory minerals that are commonly present in bauxites. As no additional sample preparation is needed, the method is an efficient means to obtain a complete set of major and

trace element data on the same sample in conjunction with XRF, which can also serve to provide concentration data for internal standards. Application of methods to reduce polyatomic interference effects may be advisable to improve measurement accuracy for elements that are sensitive to this problem such as Sc, V and Cr. The possible presence of impurities in lithium borate flux also requires attention. Future analytical work on trace elements in bauxites would benefit from the availability of more and better-characterised reference materials.

Acknowledgements

The authors would like to thank Helen de Waard for help with the LA-ICP-MS work at Utrecht University. Two anonymous reviewers provided helpful and constructive comments. This research was funded by a grant from the Suriname Environmental and Mining Foundation (SEMIF).

References

Ahmadnejad F., Zamanian H., Taghipour B., Zarasvandi A., Buccione R. and Ellahi S. (2017)
Mineralogical and geochemical evolution of the Bidgol bauxite deposit, Zagros Mountain Belt, Iran: Implications for ore genesis, rare earth elements fractionation and parental affinity. Ore Geology Reviews, 86, 755–783.

Amosova A., Panteeva S., Chubarov V. and Finkelshtein A. (2016)
Determination of major elements by wavelength-dispersive X-ray fluorescence spectrometry and trace elements by inductively coupled plasma-mass spectrometry of igneous rocks from the same fused sample (110 mg). Spectrochimica Acta Part B, 122, 62–68.

Andrade S., Ulbrich H., de Barros Gomes C. and Martins L. (2014)
Methodology for the determination of trace and minor elements in minerals and fused rock glasses with laser ablation associated with quadrupole inductively coupled plasma-mass spectrometry (LA-Q-ICP-MS). American Journal of Analytical Chemistry, 5, 701.

Awaji S., Nakamura K., Nozaki T. and Kato Y. (2006)
A simple method for precise determination of 23 trace elements in granitic rocks by ICP-MS after lithium tetraborate fusion. Resource Geology, 56, 471–478.

Bárdossy G. and Aleva G.J.J. (1990)
Lateritic bauxites. Developments in economic geology, 27 Elsevier Science (Amsterdam), 648pp.

Bédard L.P. and Barnes S.J. (2002)
A comparison of N-type semi-planar and coaxial INAA detectors for 33 geochemical reference samples. Journal of Radioanalytical and Nuclear Chemistry, 254, 485–497.

Borra C., Pontikes Y., Binnemans K. and van Gerven T. (2015)
Leaching of rare earths from bauxite residue (red mud). Minerals Engineering, 76, 20–27.

Butt C. (1986)
Vertical distribution of trace elements in laterite soil (Suriname-Discussion). Chemical Geology, 56, 159–163.

Boulangé B. and Colin F. (1994)
Rare earth element mobility during conversion of nepheline syenite into lateritic bauxite at Passa Quatro, Minais Gerais, Brazil. Applied Geochemistry, 9, 701–711.

Chen S., Wang X., Niu Y., Sun P., Duan M., Xiao Y., Guo P., Gong H., Wang G. and Xue Q. (2017)
Simple and cost-effective methods for precise analysis of trace element abundances in geological materials with ICP-MS. Science Bulletin, 62, 277–289.

Cotta A.J.B. and Enzweiler J. (2011)
Classical and new procedures of whole rock dissolution for trace element determination by ICP-MS. Geostandards and Geoanalytical Research, 36, 27–50.

da Costa M.L., da Silva Cruz G., de Almeida H.D.F. and Poellmann H. (2014)
On the geology, mineralogy and geochemistry of the bauxite-bearing regolith in the lower Amazon basin: Evidence of genetic relationships. Journal of Geochemical Exploration, 146, 58–74.

De Madinabeita G., Lorda S. and Ibarguchi G. (2008)
Simultaneous determination of major to ultratrace elements in geological samples by fusion-dissolution and inductively coupled plasma-mass spectrometry techniques. Analytica Chimica Acta, 625, 117–130.

Eggins S. (2003)
Laser ablation ICP-MS analysis of geological materials prepared as lithium borate glasses. Geostandards Newsletter: The Journal of Geostandards and Geoanalysis, 27, 147–162.

Evans E. and Giglio J. (1993)
Interferences in inductively coupled plasma-mass spectrometry. A review. Journal of Analytical Atomic Spectrometry, 8, 1–18.

Gao S., Lui X., Hattendorf B., Günther D. and Hu S. (2002)
Determination of forty-two major elements in USGS and NIST SRM glasses by laser ablation-inductively coupled plasma-mass spectrometry. Geostandards Newsletter: The Journal of Geostandards and Geoanalysis, 26, 181–196.

Govindaraju K. (1994)
1994 compilation of working values and sample description for 383 geostandards. Geostandards Newsletter, 18 (Special Issue), 158pp.

references

Govindaraju K. (1995)
1995 Working values with confidence limits for twenty-six CRPG, ANRT and IWG-GIT geostandards. Geostandards Newsletter, 19 (Special Issue), 32pp.

Grant C., Lalor C. and Vutchkov M. (2005)
Comparison of bauxites from Jamaica, the Dominican Republic and Suriname. Journal of Radioanalytical and Nuclear Chemistry, 266, 385–388.

Gu J., Huang Z., Fan H., Ye L. and Jin Z. (2013)
Provenance of lateritic bauxite deposits in the Wuchuan-Zheng'an-Daozhen area, Northern Guizho Province, China: LA-ICP-MS and SIMS U-Pb dating of detrital zircons. Journal of Asian Earth Sciences, 70, 265–282.

Günther D., von Quadt A., Wirz R., Cousin H. and Volker D. (2001)
Elemental analyses using laser ablation-inductively coupled plasma-mass spectrometry (LA-ICP-MS) of geological samples fused with $Li_2B_4O_7$ and calibrated without matrix matched standards. Mikrochimica Acta, 136, 101–107.

Horbe A.M.C. and Anand R.R. (2011)
Bauxite on igneous rocks from Amazonia and southwestern of Australia: Implication for weathering process. Journal of Geochemical Exploration, 111, 1–12.

Horbe A.M.C. and Da Costa M.L. (1999)
Geochemical evolution of a lateritic Sn–Zr–Th–Nb–Y–REE-bearing ore body derived from apogranite: The case of Pitinga, Amazonas—Brazil. Journal of Geochmeical Exploration, 66, 339–351.

Jochum K.P., Willbold M., Stoll B. and Herwig K. (2005)
Chemical characterization of the USGS reference glasses GSA-1G, GSC-1G, GSD-1G, GSE-1G, BCR-2G, BHVO-2G and BIR-1G using EPMA, ID-TIMS, ID-ICP-MS and LA-ICP-MS. Geostandards and Geoanalytical Research, 29, 285–302.

Jochum K.P., Stoll B., Herwig K. and Willbold M. (2007)
Validation of LA-ICP-MS trace element analysis of geological glasses using a new solid state 193 nm Nd:YAG laser and matrix-matched calibration. Journal of Analytical Atomic Spectrometry, 22, 112–121.

Jochum K.P., Weis U., Schwager B., Stoll B., Wilson S., Haug G., Andreae M. and Enzweiler J. (2016)
Reference values following ISO guidelines for frequently requested rock reference materials. Geostandards and Geoanalytical Research, 40, 333–350.

Korotev R. (1996)
A self-consistent compilation of elemental concentration data for 93 geochemical reference samples. Geostandards Newsletter, 20, 217–245.

Leite T., Escalfoni R., da Fonseca T. and Miekely N. (2011)
Determination of major, minor and trace elements in rock samples by laser ablation inductively coupled plasma spectrometry: Progress in the utilization of borate glasses as targets. Spectrochimica Acta Part B, 66, 314–320.

Longerich H.P., Jackson S.E. and Günther D. (1996)
Laser ablation inductively coupled plasma-mass spectrometric transient signal data acquisition and analyte concentration calculation. Journal of Analytical Atomic Spectrometry, 11, 899–904.

Mason P. and Kraan W. (2002)
Attenuation of spectral interferences during laser ablation inductively coupled plasma-mass spectrometry (LA-ICP-MS) using an rf only collision and reaction cell. Journal of Analytical Atomic Spectrometry, 17, 858–867.

May T.W. and Wiedmeyer R.H. (1998)
A table of polyatomic interferences in ICP-MS. Atomic Spectroscopy, 19, 150–155.

McLennan S. (2001)
Relationships between trace element composition of sedimentary rocks and upper continental crust. Geochemistry, Geophysics, Geosystems, 2, 4.

Miliszkiewicz N., Walas S. and Tobiasz A. (2015)
Current approaches to calibration of LA-ICP-MS analysis. Journal of Analytical Atomic Spectrometry, 30, 327–338.

Mongelli G., Boni M., Buccione R. and Sinisi R. (2014)
Geochemistry of the Apulian karst bauxites (southern Italy). Chemical fractionation and parental affinities. Ore Geology Reviews, 63, 9–21.

Monsels D.A. (2016)
Bauxite deposits in Suriname: Geological context and resource development. Netherlands Journal of Geosciences - Geologie en Mijnbouw, 95, 405–418.

Monsels D.A. and Van Bergen M.J. (2017a)
Bauxite formation on Proterozoic bedrock in Suriname. Journal of Geochemical Exploration, 180, 71–90.

Monsels D.A. and Van Bergen M.J. (2017b)
Bauxite formation on Tertiary sedimentary parent rocks in Suriname. Journal of Geochemical Exploration, 180, 71–90.

Mordberg L.E., Stanley C.J. and Germann K. (2001)
Mineralogy and geochemistry of trace elements in bauxites: The Devonian Schugorsk deposit, Russia. Mineralogical Magazine, 65, 81–101.

Nesbitt R., Hirata T., Butler I. and Milton J. (1997)
UV laser ablation ICP-MS: Some applications in the Earth sciences. Geostandards Newsletter: The Journal of Geostandards and Geoanalysis, 20, 231–243.

Ochsenkühn-Petropoulou M., Ochsenkühn K. and Luck J. (1990)
Comparison of inductively coupled plasma-mass spectrometry with inductively coupled plasma atomic emission spectrometry and instrumental neutron activation analysis for the determination of rare earth elements in Greek bauxites. Spectrochimica Acta, 46, 51–65.

Ochsenkühn-Petropoulou M., Lyberopulu T. and Parissakis G. (1994)
Direct determination of lanthanides, yttrium and scandium in bauxites and red mud from alumina production. Analytica Chimica Acta, 296, 305–313.

references

Orihashi Y. and Hirata T. (2003)
Rapid quantitative analysis of Y and REE abundances in XRF glass bead for selected GSJ reference rock standards using Nd-YAG 266 nm UV laser ablation ICP-MS. Geochemical Journal, 37, 401–412.

Panteeva S., Gladkochoub D., Donskaya T., Markova V. and Sandimirova G. (2003)
Determination of 24 trace elements in felsic rocks by inductively coupled plasma-mass spectrometry after lithium metaborate fusion. Spectrochimica Acta Part B, 58, 341–350.

Paramguru R., Rath P. and Misra V. (2004)
Trends in red mud utilization – A review. Mineral Processing and Extractive Metallurgy Review, 26, 1–29.

Park J., Al-Mutairi A., Yoon S., Mochida I. and Ma X. (2016)
The characterization of metal complexes in typical Kuwait atmospheric residues using both GPC coupled with ICP-MS and HT GC-AED. Journal of Industrial and Engineering Chemistry, 34, 204–212.

Petrelli M., Perugini D., Poli G. and Peccerillo A. (2007)
Graphite electrode lithium tetraborate fusion for trace element determination in bulk geological samples by laser ablation ICP-MS. Microchimica Acta, 158, 275–282.

Reed N., Cairns R., Hutton R. and Takaku Y. (1994)
Characterization of polyatomic ion interferences in inductively coupled plasma-mass spectrometry using a high-resolution mass spectrometry. Journal of Analytical Spectrometry, 9, 881–896.

Regnery J., Stoll B. and Jochum K.P. (2009)
High-resolution LA-ICP-MS for accurate determination of low abundance of K, Sc and other trace elements in geological samples. Geostandards and Geoanalytical Research, 34, 19–38.

Sampaio G.M.S. and Enzweiler J. (2015)
New ICP-MS results for trace elements in five iron-formation reference materials. Geostandards and Geoanalytical Research, 3, 105–119.

Shazzo Y. and Karpov Y. (2016)
Laser sampling in inductively coupled plasma-mass spectrometry in the inorganic analysis of solid samples: Elemental fractionation as the main source of errors. Journal of Analytical Chemistry, 71, 1069–1080.

Topp S., Salbu B., Roaldset E. and Jørgensen P. (1984)
Vertical distribution of trace elements in laterite soil (Suriname). Chemical Geology, 47, 159–174.

Totland M. and Jarvis K. (1993)
Determination of the platinum-group elements and gold in solid samples by slurry nebulisation ICP-MS. Chemical Geology, 104, 175–188.

Ujaczki E., Zimmermann Y., Gasser C., Molnár Feigl V. and Lenz M. (2017)
Red mud as secondary source for critical raw materials-extraction study. Journal of Chemical Technology and Biotechnology, 92, 2835–2844.

Vukotić P. (1983)
Determination of rare earth elements in bauxites by instrumental neutron activation analysis. Journal of Radioanalytical and Nuclear Chemistry, 78, 105–115.

Wang X., Jiao Y., Du Y., Ling W., Wu L., Cui T., Zhou Q., Jin Z., Lei Z. and Weng S. (2013)
REE mobility and Ce anomaly in bauxite deposit of WZD area, Northern Guizhou, China. Journal of Geochemical Exploration, 133, 103–117.

Whitty-Léveillé L., Drouin E., Constantin M., Bazin C. and Larivière D. (2016)
Scandium analysis in silicon-containing minerals by inductively coupled plasma tandem mass spectrometry. Spectrochimica Acta Part B, 188, 112–118.

Yu Z., Norman M. and Robinson P. (2003)
Major and trace element analysis of silicate rocks by XRF and laser ablation ICP-MS using lithium borate fused glasses: Matrix effects, instrument response and results for international reference materials. Geostandards Newsletter: The Journal of Geostandards and Geoanalysis, 27, 67–89.

Zhang J., Deng Z. and Xu T. (2005)
Experimental investigations on leaching metals from red mud. Light Metals, 2, 13–15.

Zhang W., Qi L., Hu Z., Zheng C., Lui Y., Chen H., Gao S. and Hu S. (2016)
An Investigation of digestion methods for trace elements in bauxite and their determination in ten bauxite reference materials using inductively coupled plasma-mass spectrometry. Geostandards and Geoanalytical Research, 40, 195–216.